CHAPTER 2

LITERATURE REVIEW

The macrocyclic ligand is defined as a cyclic molecule with three or more potential donor atoms. The heteroatom ring must consist of at least nine atoms. Referring to the donor type, macrocyclic ligands are categorized into oxocrown ether for oxygen donor atoms, azacrown ether for nitrogen donor atoms or mixed donor atoms. The most diverse and highlighted class is aza crown discovered by Curtis in 1960's (Chandra et al., 2005). Ligand containing nitrogen has a tendency predominantly to form a coordination bond with transition metal ions (Bowman-James, 2006). Besides, nitrogen may interact with many types of organic compound and inorganic complex anions easily. The significance of tetraaza macrocyclic ligand has been studied thoroughly by focusing on its complexation towards a variety of metal ions (Prakash et al., 2014). This is because tetraaza macrocyclic possess high selectivity properties, has strong possibility to be applied in the area of waste treatment to remove toxic metals (Yusuf et al., 2019), as a contrast agent in medical imaging (Clough et al., 2019) and as anti-cancer (El-Boraey et al., 2015).

Since neutral tetraaza macrocyclic ligand was introduced by Curtis, their metal complexes have been prepared by metal template reaction under refluxed conditions. Later, a remarkable discovery of the same ligand but in a protonated form showing the NH_2 group at a diagonal position of the tetraaza group prepared by the non-template method (Yamin et al., 2012). **Figure 2.1** compares the molecular structure between neutral and protonated tetraaza macrocyclic ligand. Further investigation was conducted

on protonated tetraaza macrocyclic ligand with bromide, chloride, perchlorate, nitrate, hexafluorophosphate counter anions and their biological activities (S. F. M. Yusoff et al., 2013). From the experiment, macrocyclic bromide and macrocyclic perchlorate salts were more effective against gram- positive E. Faecalis and gram-negative E.Coli.

The attachment between the metal ion and its ligand is due to Lewis acid-base interaction forming a macrocyclic compound (Hosmane, 2017). Central metal ion acts as Lewis acid often accepting lone pairs from Lewis base which is the ligand to form a dative bond. A metal ion is located at the centre of the macrocyclic ligand and the combination of them is known as the macrocyclic complex.

The discovery of protonated tetraazamacrocylic salts prepared using a novel non-template method has enabled the detailed study on the complexation reaction with various transition metal ions such as copper, nickel, and zinc complexes were carried out (S. F. M. Yusoff, 2015). Differ from the metal template reaction, the non-template method synthesizes the ligand first, then combines it with transition metal ion and transforms it into a complex compound. Based on the X-ray crystallography, the central metal ion formed coordination bonds to the four nitrogen atoms, exhibits square planar geometry as in **Figure 2.2**. The cationic charge of the complex was balanced with anion from the macrocyclic ligand. While the deprotonation of the azomethine group produces acid/base complex with the metal salt. The biological studies gave significant results where macrocyclic complexes showed greater antibacterial activity than their respective free ligands.

The success of non-template synthesis macrocyclic compound allows this study to expand the complexation reaction of protonated tetraaza macrocyclic ligand with second-row of a transition metal which is Pd (II) through computational approach. Compared to the organic species, the square-planar metal complexes have excellent

electron-donating ability which is expected to demonstrate non-linear optical behaviour (Fackler, 1999). Thus, motivation for this theoretical study is to predict the structural geometry, understand metal-ligand interaction at ground state, and explore the optical properties of Pd(II) tetraaza macrocylic complex at excite state in solvent surrounding for future optoelectronic application.

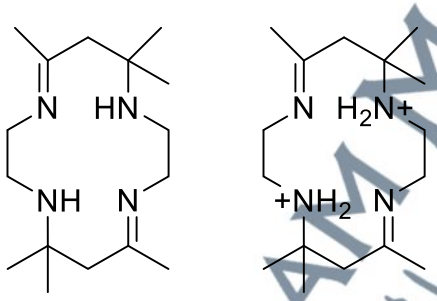

Figure 2.1: Neutral (left) and Protonated (right) 14-Membered Tetraaza Macrocyclic Ligand

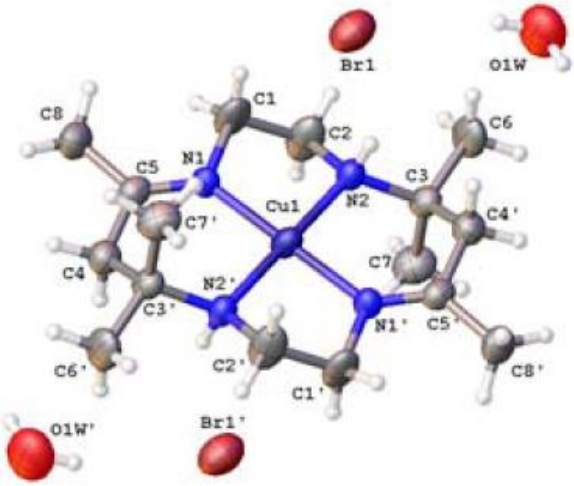

Source: Yusoff et al. (2015)

Figure 2.2: Molecular structure of cation Cu(II) tetraaza macrocyclic complex with bromide counter anion drawn at 50% probability ellipsoids (reprinted from reference with permission from authors)

2.1 Structural and Electronic Properties of Tetraaza Macrocyclic Ligand

2.1.1 Geometry Optimization

To date, there have been many studies on synthesizing tetraaza macrocyclic ligand with different first-row transition metals via non-template synthesis (Yusoff et al., 2015). Although the binding of first-row transition metals to this ligand has been extensively researched, the binding of second-row transition metals is still relatively unexplored. It has been demonstrated that the larger size of second-row transition metals may potentially affect their binding to tetraaza macrocyclic ligands (Hay et al., 2001). Achieving optimal complementarity requires the metal ion to contact all donor atoms of the ligand at an ideal distance. If the array of donor atoms creates a cavity that is too large, some donor atoms may not be in contact. Conversely, if the cavity is too small, the metal ion cannot contact the donors at the optimal distance. The concept of size-matching the ligand cavity to the size of the metal ion has been an important consideration in past and present ligand design.

To further illustrate the concept, a theoretical study was conducted to figure out the interaction between oxygen and tetraaza macrocyclic manganese complexes (Costa et al., 2016). The optimization of manganese-tetraaza[14]annulene (MnTAA) structure was performed using the B3LYP hybrid functional and LanL2TZ basis set. The optimized structure of MnN_4 complexes achieved stability with minimal potential energy and formed square planar geometry. The angle between nitrogen atoms and manganese ion is 180^o confirming that Mn was presented in the nitrogen atoms plane of the complexes.

Besides, the DFT study on Pd(II) complexes by using PBE functional in gas phase determines the value of Pd-N bond length were approximately 1.9 – 2.1 Å and bond angles 80 – 100 ^{o} (Bandyopadhyay et al., 2016). The sum of each angle around

the Pd central approximately 360° indicates the geometry of oxime based ligand with Pd(II) complex is square planar with dsp^2 hybridisation.

The crystal structure of $C_{14}H_{24}N_8Pd_2$ was investigated by Kwang Ha (Ha, 2017), revealing a cationic Pd(II) complex $[Pd(cyclam)]^{2+}$ and an anionic Pd(II) complex $[Pd(CN)_4]^{2-}$. Each Pd(II) ion was found to be coordinated by either N_4 atoms from the tetradentate cyclam ligand or C atoms from four CN− ligands, respectively, in slightly distorted square-planar environments. The bond lengths for Pd—N and Pd—C were found to be almost equal, measuring (Pd—N) = 2.0447–2.0459 Å and Pd—C = 1.9955–2.007 Å, respectively. The cationic and anionic complexes were linked by intermolecular N—H···N_4(cyanido) hydrogen bonds, forming a three-dimensional network.

The information on structural geometry provides insights into how the metal ion can effectively bind to the macrocyclic ligand and form diverse cationic and anionic complexes. Therefore, this research conducted a structural and electronic analysis to confirm how the larger size of second-row transition metal, specifically the Pd(II) ion, binds to the new structure of the protonated tetraaza macrocyclic ligand that was synthesized using a non-template method.

2.1.2 Natural Bond Orbital Analysis

One of the useful applications of DFT is estimating the occupancies of localized centre orbitals and analysing all the possible interactions between delocalized electrons and natural bond type orbitals (NBO).

NBO is the calculated localized bonding orbitals that have a maximum quantity of electron density in a molecular system. There are three classes of NBO orbitals:

- Lewis-type orbital, L consist of σ and π bonding or lone pair

- Non Lewis-type orbital, NL which is unoccupied antibonding
- Rydberg orbital, R that is located outside the atomic valence shell.

The NBO population analysis of 1-Azanapthalene-8-ol was conducted by Rubarani and the team to observe intermolecular interaction in terms of charge transfer and orbital occupancy (Gangadharan, 2014). The calculated natural orbitals showed that π(C9-O11) bonding is formed from the hybridization of sp^3 on oxygen (mixture of 24.21% *s*, 75.60% *p* and 0.18% *d*). The occupancy of σ (C9-O11) bond is 1.9922 followed by σ(O11-H18) bond occupancy 1.9909 indicates these orbitals have the maximum electron density distribution. Hence more interactions of carbon with oxygen and hydrogen groups may occur contributing to the stability and strength of molecules.

Furthermore, the second-order disturbance theory was applied to examine the interactions among electron donor orbital and acceptor and to determine the value of stabilization energy, $E^{(2)}$ value (Kumar et al., 2015). A larger value of $E^{(2)}$ indicates that there is more interaction between donor-acceptor electrons and a higher extent of conjugation in the system. In the case of 1-Azanapthalene-8-ol , the transition of lone pair from LP(1)C10 $\rightarrow \pi^*$(C8-C9) antibonding resulted in an energy of stabilization, 83.18 kJ/mol, leading to the conformation of a carbon ring.

In terms of metal complex, PdL_2 where L= 2-allyliminomethyl phenolate was synthesized to investigate the structural and electronic properties (Guelai et al, 2018). The NBO analysis reveals central metal ion coordinates to the ligands because of electron donation from lone pairs on nitrogen and oxygen atoms to palladium orbitals (*s* and *d*). Therefore, calculated stabilization energy during the transition of (2*s*2*p*)N $\rightarrow$ ($d_{x^2-y^2}$)Pd : 72.37 kcal/mol and (2*s*2*p*)N $\rightarrow$ (*s*)Pd : 38.93 kcal /mol is very high.

Besides, another significant found during transitions of $\pi_{C=C} \rightarrow \pi^*_{C=C}$ and $LP(O) \rightarrow \pi^*_{C-C}$ for the formation of aromatic rings of the ligands.

From the literature, NBO analysis successfully showed electron transfer from donor group of natural compound very helpful in stabilizing the natural compound. Hence, this analysis should be conducted on protonated tetraaza macrocyclic compound and its complex to identify their hybridization orbitals and which donor groups will give more stabilization to the molecules.

2.1.3 Molecular Electrostatic Potential Surface

The molecular electrostatic potential surface (MEPS) is a graphical representation of the electrostatic potential distribution on the surface of a molecule. It is a useful tool in computational chemistry that allows the visualization of regions of high and low electron density on the molecular surface, and it can be used to predict the reactivity of a molecule by identifying electrophilic and nucleophilic regions. The MEPS is calculated using quantum mechanical methods, such as density functional theory (DFT), and it provides important information about the electronic properties and behaviour of a molecule. (Sheikhi et al., 2014).

The electrostatic potential of a molecule is influenced by the electronic distribution within the molecule, which is in turn determined by the atoms' charges and positions. Negative electrostatic potential regions in a molecule are caused by an attraction of protons towards concentrated electron density, such as lone pairs and π bonds. This negative potential region is suitable for nucleophilic attacks (Joshi et al., 2013). The positive electrostatic potential regions in a molecule, on the other hand, result from a lack of electrons in a particular area, making it more attractive to electrons. This region is suitable for electrophilic attacks.

In molecular electrostatic potential surface (MEPS), the red colour represents the region with the most negative electrostatic potential, the blue colour represents the region with the most positive electrostatic potential, and the green colour represents regions with zero or neutral electrostatic potential. The value of electrostatic potential is different on the surface represented by different colours in the order from electron-rich to electron-deficient: red < orange < yellow < green < blue colour (Drissi et al., 2019).

The effect of ligand modification on the structure of tetraazamacrocyclic complexes Au(III) has been investigated using MEPS analysis (Kryuchkova, 2021). In a mono-protonated complex, $[Au(C_{14}H_{23}N_4)]^{2+}$ the most negative potential regions are localized on the N and C atoms. However, when two H^+ ions are added to the di-protonated complex, $[Au(C_{14}H_{24}N_4)]^{3+}$ all region of the complex become completely blue because shielded by positive potential.

In another investigation, electronic properties of pyrazolo-pyridine derivatives, specifically (3,5-dimethyl-4-(3-nitrophenyl)-1,4,7,8-tetrahyddrodipyrazolopyridine), were studied as a potential corrosion inhibitor using a theoretical approach (Dohare et al., 2019). The molecular electrostatic potential surface (MEPS) analysis provided clear information about the electropositive potential distribution of the natural compounds, where the negative region is concentrated primarily over the N atoms of the pyrazolo-pyridine rings and the NO_2 group of the benzene ring. The protonated compound, on the other hand, showed a deep blue region all over the ring, indicating a low electron distribution and a decreased tendency for electron donation.

Based on previous studies, it can be inferred that the protonation and deprotonation of a molecule can influence the nitrogen group's ability to donate and accept electrons. Therefore, conducting MEPS analysis on the protonated

tetraazamacrocylic ligand and its metal complex can provide insights into the effect of electropositive potential during complexation with Pd(II) ion.

2.2 Optical Properties of Tetraaza Macrocyclic Ligand

2.2.1 Frontier Molecular Orbital Study

Frontier molecular orbital, FMO theory is used to determine the energy change in molecular orbitals. Two types of molecular orbitals that are involved are the highest occupied molecular orbital, HOMO and the lowest unoccupied molecular orbital, LUMO. FMO explained the charge transferred and the energy difference between HOMO and LUMO termed as an energy gap, E_{gap}.

$$E_{gap} = E_{LUMO} - E_{HOMO} \quad (1)$$

The E_{gap} between these two orbitals can predict the strength and stabilization of transition metal complexes and colour generated in solution (Griffith et al., 1935). The smallest energy gap of orbitals leads to high reactivity and consequently lowers the stabilization of the compound (Ali et al., 2018).

Gokhan and co-workers studied the FMO of a macrocyclic compound, Pyr-2-Bt-$PdCl_2$ and its HOMO-LUMO is illustrated in **Figure 2.3** (Dikmen, 2019). HOMO exhibit π bonding as electron donor while LUMO as acceptor exhibit π^* antibonding characteristic. The energy gap between the ground state and the excited state, LUMO, is 1.04 eV, which represents the energy needed for an electron to move to higher states. The transition of the lone pair of nitrogen atoms near the pyridine ring from the HOMO to the LUMO orbitals, towards the Pd and Cl atoms, increases the stability of the molecule. Consequently, it can be concluded that the active site for a reaction is located in the vicinity of the pyridine rings, owing to the presence of electron donors.

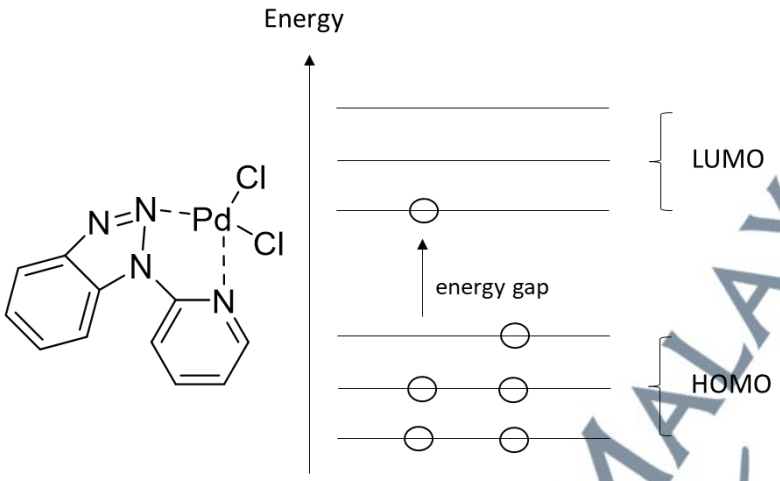

Source: Dikmen (2019)

Figure 2.3: Frontier molecular orbital of Pyr-2-Bt-$PdCl_2$

The atomic arrangement may affect the E_{gap} as reported by Sen and teams (Şen et al., 2013). Firstly, they synthesized open ring tetraazamacrocycles, 2-Amino-N-[3-[(2-aminobenzoilamino)propil] benzamide having a gap 0.185 eV. Upon dissolution in diethyl malonate, the Okso4Bzo2[16]dien-N4 underwent ring closure, resulting in a smaller energy gap of 0.136 eV. This reduced energy gap corresponds to the minimum excitation energy required for the transfer of electron charge in the ligand.

The study conducted by Gammal in 2018 reported that the tetraaza macrocyclic ligand with porphyrin group exhibited negative energy gap of HOMO and LUMO orbitals, indicating stability of the product (El-Gammal et al., 2018). The nitrogen donor groups were identified as preferred sites for nucleophilic attack. The large energy gap of 2.586 eV suggested high excitation energies and good stability of the ligand, while a smaller energy gap suggested higher reactivity and likelihood of charge transfer.

The previous study suggests that a small energy gap of Pd(II) complexes is 1.04 eV while energy gap of tetraaza macrocyclic ligand between 2.586-0.136 eV as summarize in **Table 2.1**. In line with this, the current research aims to conduct frontier

molecular orbital analysis on tetraaza macrocyclic ligand and its complex to identify a small energy gap that is suitable for optoelectronic technology. This analysis will provide insights into the electronic properties and potential applications of the complex in various fields such as solar cells, sensors, and electronic devices.

Table 2.1: Summary of Findings on Energy Gap of Tetraaza Macrocyclic Complex

Structural Compound	Energy gap (eV)	References
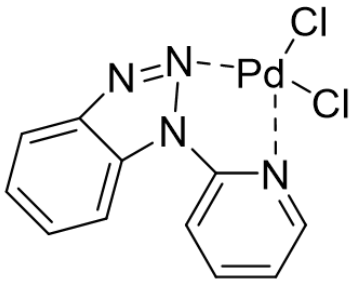	1.040	(Dikmen, 2019)
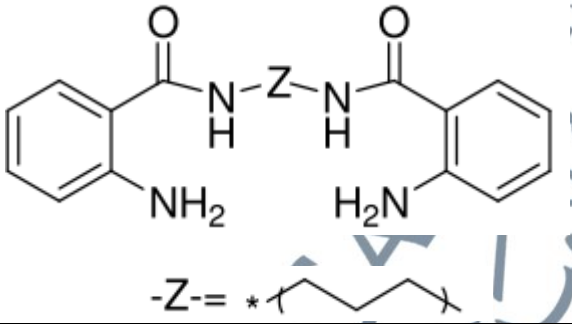	0.185	(Şen, 2013)
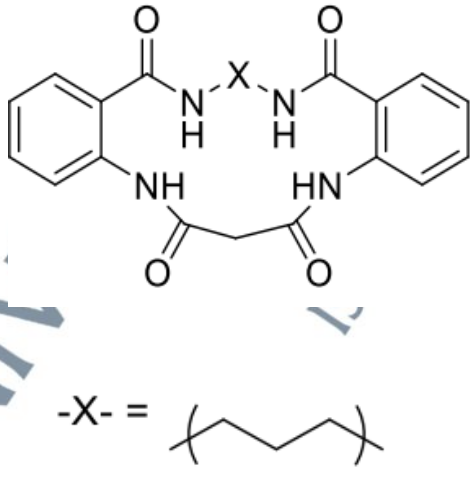	0.136	(Şen, 2013)

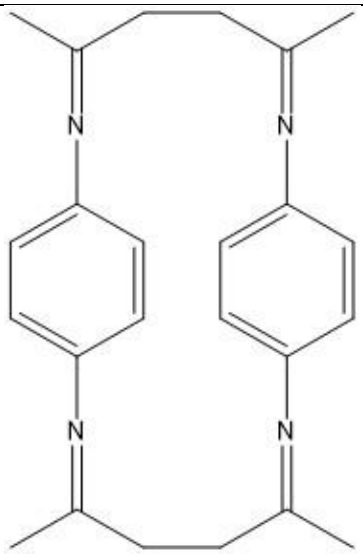	2.586	(El-Gammal, 2018)

2.2.2 UV-VIS Spectroscopy

UV-VIS spectroscopy is an effective analytical tool to study the optical properties of substances such as liquid or solid. This technique measures the transmittance, reflection and absorption of light across the intended optical range. When an electron absorbs energy, it can move from a lower energy level (usually a bonding orbital) to a higher energy level (usually an anti-bonding orbital). This transition leads to the formation of an excited state molecule with a higher energy than the ground state molecule. The energy required to make this transition corresponds to a specific wavelength of light, which can be observed as an absorption peak in the UV-Vis absorption spectrum of the molecule (Seekaew, 2014) as in **Figure 2.4**. The UV-visible absorption spectrum displays the absorbance which measures the amount of light absorbed versus wavelength of light (Clark, 2016). We can determine which wavelengths of light are being absorbed by the molecule and identify the molecule based on the characteristic wavelengths at which the transition of electrons occurs. The higher the value of absorbance at a specific wavelength, the more light is being absorbed

by the molecule at that wavelength, indicating a stronger absorption of light and a higher probability of electronic transitions occurring at that energy level.

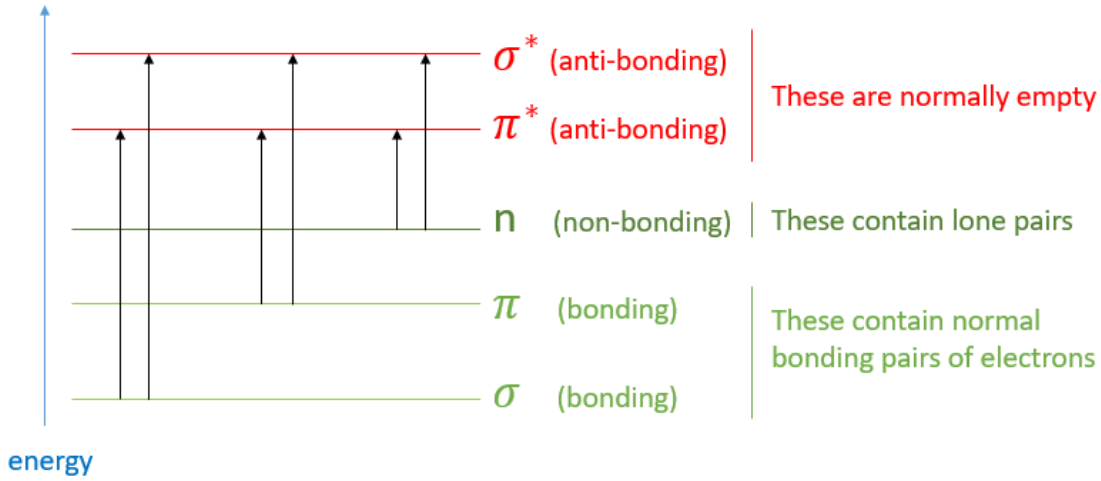

Figure 2.4: The Possible Electron Transition from Full Orbital to Empty Orbital

According to (Ahmad et al., 2020), the tetradentate ligand exhibits a simulated electronic absorption with a maximum wavelength of 327 nm, which is attributed to the n-π* electronic transition of the imine chromophore. This transition involves the movement of electrons from the non-bonding orbital, n, to the anti-bonding orbital, π*. Upon complexation with a Pd(II) atom, the maximum absorption peak shifts to a higher wavelength of 410 nm due to the weakening of the C=N bond, as the lone pair of electrons on nitrogen is donated to the Pd(II) atom during the metal-ligand interaction.

Besides, a singlet excited state study on Pd(II) complex with tetramethyl Schiff base ligand identified a weak bond at 447 nm corresponding to the ligand-ligand charge transfer attribute (Brahim, 2019). The weak bond shows that transition in the complex does not involve *d*-metal orbitals because of the lack of charge transfer characteristic.

However, in another study Pd(II) complex with different Schiff base ligand (2-allyliminomethyl-4-methyl phenolate) exhibit metal-ligand interaction where a

transition is observed around 280 nm assigned from d_{Pd} and $\pi_{phenolate}$ to $\pi^*_{phenolate}$ orbital (Guelai et al., 2018).

In separate study, di-nuclear Pd(II) complex with 1,4,8,11-tetrakis(2-p-toluenesulfonamidoethyl)-1,4,8,11-tetraazacyclotetradecane, [Pd2(tstaec)], was synthesized and characterized by UV–vis spectroscopies to analyse the complex's electronic properties (Wada et al., 2008). The spectrum showed a strong band at 230 nm, which may indicate charge-transfer transitions, along with shoulders at 266 and 330 nm. Additionally, broad absorptions were observed around 415 and 443 nm, which could be associated with *d-d* transitions. These spectral features are consistent with a square-planar Pd(II) ion surrounded by N_4 donor atoms. To further understand the electronic transitions responsible for the observed UV-vis spectra, TD-DFT calculations were performed using the Gaussian program suite. The calculated transitions at 487, 416, and 330 nm were found to correspond well with the experimental bands at 443, 415, and 330 nm, respectively. Moreover, the calculated transitions at 281 and 259 nm were assigned to the experimental shoulder bands at 266 nm. Overall, the calculated values showed a general resemblance to the experimental spectra, providing insight into the electronic properties of the dinuclear Pd(II) complex with macrocyclic ligand.

Another fascinating finding, Sanjeevani synthesized and characterized complexes of lanthanide groups Ce(III), Pr(III), Nd(III), Sm(III), Gd(III), and Eu(III) with an orthophenyl diamine-containing nitrogen donor [N4] macrocyclic ligand with a 14-membered backbone (Shankarwar et al., 2015). The electronic spectra of these complexes were recorded in DMSO, and the data indicates that the intense charge transfer bands were observed in all the complexes, and most of the absorption arising from weak *f-f* transition. The complexes exhibited two transitions in the range of 350-380 nm due to charge transfer transition and 400-430 nm due to *f-f* transition.

Macrocyclic ligands with N_4 donor atoms have been found to be highly selective for binding with larger metal ions, such as lanthanides, due to their size and charge density. The ligand can effectively encapsulate the metal ion within its cavity, providing a highly stable and coordinated complex.

The solute-solvent interaction shows a significant solvent effect on the optical absorption spectra of $Au_{13}L_8^{3+}$ as per conducted by Machado, using B3LYP hybrid functional, LANL2DZ basis set and C-PCM implicit solvation model (Machado, 2019). The absorption spectra of $Au_{13}L_8^{3+}$ exhibit similar trends, with a hypsochromic shift observed around 200-300 nm with an increase in solvent polarity from gas to water. On the other hand, a progressive bathochromic shift was observed around 400-600 nm of $Au_{13}L_8^{3+}$ as the solvent polarity increased from non- polar solvents like hexane, toluene, and THF to polar solvents like DCM, ethanol, and water.

Therefore, the structural geometry of the ligand and its complex, as well as the polarity of the solvent, can affect the absorption spectra of the system. When a transition metal is present, it can promote the mobility of electrons, leading to changes in the absorption spectra. On the other hand, the polarity of the solvent can cause shifts in the absorption spectra due to the different levels of solvation of the system.

2.2.3 Non-Linear Optical Study

Non-linear optical, NLO is a study to understand the interaction of the intense light beam with the material system in response to the applied optical source. The NLO phenomenon occurs when a high-intensity beam of light, such as a laser, strikes a medium and induces a dipole moment per unit volume, which is known as electric polarization. At this time, the relationship between electric field, E, and polarization, P is no longer linear, the non-linear effect takes place and its parameters such as phase, frequency, amplitude or polarization are changed. It was first discovered by Franken

through second harmonic generation, SHG when he observed the frequency of transmitted light in the ultraviolet region was twice the frequency of the incident light, and the wavelength was half that of the incident light (Franken et al., 1961). As in **Figure 2.5**, a single photon is converted into two photons with twice the energy and half the wavelength (i.e., twice the frequency) of the original photon. This is a result of the interaction between the incident light and the electrons in the material, which causes the electrons to oscillate at twice the frequency of the incident light, producing the second harmonic. The two photons produced by the SHG process are typically emitted at an angle to the original photon, which allows them to be easily separated and detected.

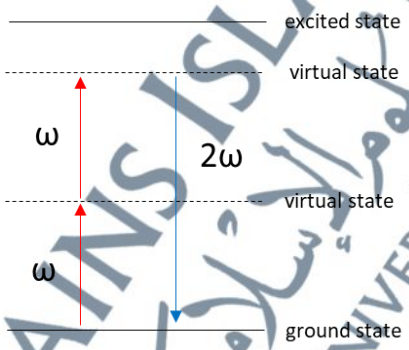

Figure 2.5: Illustration of Second Harmonic Generation

Since the applied electric field perturbed the separation between electric charges (dipole moment) of the non-linear material, the optical parameters are calculated to characterize the SHG process. The important parameters are (Asselberghs et al., 2006):

- $\chi^{(2)}$: Second-order nonlinear susceptibility
- $\beta^{(2)}$: First hyper-polarizability
- μ: Dipole moment

Liu and his team investigated the second-order nonlinear properties of Schiff-base M(II) (M=Ni,Pd,Pt) complexes (Liu, 2006). Schiff-base is a compound with

general structure $R_2C=NR'$ ($R' \neq H$) used as the ligand to form coordination complexes with metal ions. The research study explores a series of mono Schiff-base M(II) complexes where M can be Ni, Pd, or Pt. The complexes were investigated using donor/acceptor exchange, metal substitution, and NH3σ-ancillary as the ligand (**Figure 2.6**).

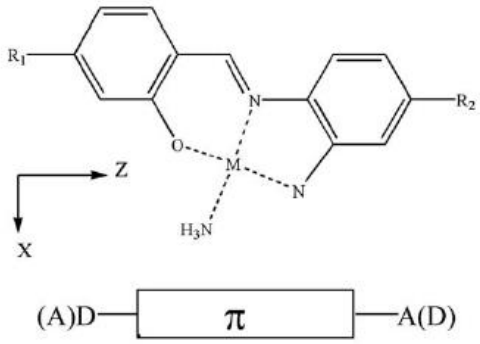

1a: $R_1=-N(C_2H_5)_2$, $R_2=-CH_2C(CN)_2$, M=Ni.
1b: $R_1=-CH_2C(CN)_2$, $R_2=-N(C_2H_5)_2$, M=Ni.
2a: $R_1=-N(C_2H_5)_2$, $R_2=-CH_2C(CN)$, M=Pd.
2b: $R_1=-CH_2C(CN)_2$, $R_2=-N(C_2H_5)_2$, M=Pd.
3a: $R_1=-N(C_2H_5)_2$, $R_2=-CH_2C(CN)$, M=Pt.
3b: $R_1=-CH_2C(CN)_2$, $R_2=-N(C_2H_5)_2$, M=Pt

Source: Liu (2006)

Figure 2.6: Structural Formulas for Mono Schiff-Base M(II) (M = Ni, Pd, Pt) Complexes

Table 2.2: The First Hyperpolarizabilities (a.u) and Dipole Moments (Debye) of All Complexes

	β_{xxx}	β_{xyy}	β_{xzz}	β_{zxx}	β_{zyy}	β_{zzz}	β_{tot}	$\lvert\mu\rvert$
1a	-402.5	85.8	2527.5	-215.8	-102.3	28119.2	27888.9	15.6
1b	-166.4	84.1	-974.1	134.8	78.6	-58167.0	57963.2	13.6
2a	-415.6	83.4	1194.9	-339.3	-91.5	29947.8	29529.6	15.3
2b	-242.8	76.4	1488.3	-7.7	87.6	-56104.9	56040.7	13.8
3a	-333.9	61.8	1081.6	-272.5	-57.3	29878.9	29560.1	15.2
3b	-144.7	56.2	1702.3	-197.1	94.9	-53863.7	53990.1	13.8

Source: Liu (2006)

The β and μ were estimated at B3LYP/LanL2DZ method using field frequency of 0.0010 a.u. β_{tot} for all metal complexes can be calculated from β components by using the equation:

$$\beta_{tot} = [(\beta_{xxx} + \beta_{xyy} + \beta_{xzz})^2 + (\beta_{yyy} + \beta_{yxx} + \beta_{yzz})^2 + (\beta_{zzz} + \beta_{zxx} + \beta_{zyy})^2]^{1/2} \quad (2)$$

From the data in **Table 2.2**, it can be concluded that the exchange of donor/acceptor influences the values of dipole moments in all metal complexes. The structures of 1a, 2a, and 3a display large dipole moments, but small β values (Wang et al,. 2019). The large dipole moments of ground state molecules would be disadvantages to the generation of NLO response. It can be testified that complex having the largest β and smallest μ exhibit high response on NLO activity. Hence, structure 1b is a great NLO material. The theoretical investigation shown the electronic structural differences are reflected in the different second-order NLO responses provide the possible application of photo-catalyst activity.

Besides, a novel [Mn(tda)(phen)] complex (tda= 1,3-Thiazolidine-2,4-dicarboxylic acid; Mn= Manganese (II); phen= 1,10 phenanthroline) has been synthesized and characterized by NLO study. The results show μ = 12.376 D and β = 41.699x10^{-30}esu which are higher than typical NLO materials (Altürk et al, 2015). The significant properties of the Mn(II) complex is due to the presence of carboxylic acid groups (negative electrostatic potential) at the opposite sides of the thiazole ring followed by a small HOMO-LUMO gap (2.17 eV) make the complex more reactive and easily polarized.

In another study, NLO analysis was conducted on tetraaza macrocyclic ligand, 1,4,7,10-tetraazacyclotetradecane-11,14-dione using DFT method (Remiya et al., 2021). The key finding of the study is that tetraaza macrocyclic ligand has a significant magnitude of nonlinear optical properties, specifically on the first-order molecular hyperpolarizability. The computed data showed that the dipole moment of tetraaza macrocyclic ligand (3.4037 D) is much higher than that of urea (1.3732 D). The static

polarizability ($23.0626x10^{-24}$ esu) and total polarizability ($6.5351x10^{-24}$ esu) of tetraaza macrocyclic ligand were also calculated and found to be relatively high. The study showed that the NLO property of the compound increased with increasing first order hyperpolarizability, static polarizability and total polarizability. The computed first-order molecular hyperpolarizability of tetraaza macrocyclic ligand $3.1196x10^{-30}$ esu was found to be significantly higher than that of standard urea $0.3728x10^{-30}$ esu. Overall, the study suggests that the presence of two amide groups in the tetraazamacrocyclic system leads to a sizable NLO response.

Since the early 20's there are consistent studies on optical properties of the organic compounds containing nitrogen groups in the solvation model using the theoretical approach. Significant discovery has been found where NLO activity strongly influenced by polarity of the solvent with proper structural design (pi-conjugated system) can lead to a large range of hyperpolarizibility values (Corozzi et al., 2009). For example, merocyanine compound with π–conjugated system has been investigated under various solvation environments (dioxane, $CHCl_3$, DMSO) using IEFPCM model (Corozzi et al., 2009). From the analysis, the compound shows average absorption energies during excitation around 2.00-2.06 eV for all solvents. While the hyperpolarizabilities (10^{-30} esu) of merocyanine compound in different solvent portrays significant changes where dioxane= 454, $CHCl_3$= 721 and DMSO= 1029.

The organometallic materials also exhibit the same behaviour in solvation models. The optical properties of thiophene acetylide Ru(II) complexes calculated by TD-DFT approach using self-consistent isodensity model (SCI-PCM) give the energy of the transition HOMO to LUMO state around 2.40-2.48 eV in different surrounding media (choloroform, acetone, and methanol) (Mendes et al., 2010). The hyperpolarizibility values (10^{-30} esu) increase as the polarity of the solvent increase

where choloroform= 229.30, acetone=290.30, and methanol=298.81. This implies the presence of metal ion in the organic compound and solvent surrounding may improve the NLO activity. All the findings are concluded in **Table 2.3**.

Table 2.3: Summary of Finding on NLO Value of Various Compund

Compound	Medium	B_{tot} (esu) ($x10^{-30}$)	References
mono Schiff-base Pd(II)	Gas	29529.6	(Liu, 2006)
Mn(tda)(phen) complex	Gas	41.699	(Altürk et al, 2015)
Tetraazacyclotetradecane	Gas	3.1196	(Remiya et al., 2021)
Urea	Gas	0.3728	
Merocyanine compound with π–conjugated system	Sioxane	454	(Corozzi et al., 2009)
	$CHCl_3$	721	
	DMSO	1029	
Thiophene acetylide Ru(II) complexes	Choloroform	229.30	(Mendes, 2010)
	Acetone	290.30	
	Methanol	298.81	

Based on literature, the 14-membered protonated tetraaza macrocyclic ligand synthesized via non-template method has gained increasing research attention. Studies have focused on the use of different ligand salts, metal salts for complexation, and biological activity against bacteria. This research aims to investigate the structural, electronic, and optical properties of Pd(II) tetraaza macrocyclic complex through a theoretical approach.. The implementation of DFT, TD-DFT, and IEFPCM analysis can give a better understanding of structural total energy, stabilization energy, metal-ligand interaction, excitation energy, molecular orbitals, and other microscopic behaviour.

CHAPTER 3

RESEARCH METHODOLOGY

Computational modelling is a mathematical model to study the behaviour of complex systems such as static and dynamic systems by using computational simulation. Computational chemistry approach can be divided to three main methods molecular mechanics, semi-empirical and quantum mechanics.

Molecular mechanics employs force fields based on classical mechanic principles to investigate the behaviour of atoms and molecules (Kollman et al., 1997). This is accomplished by utilizing a molecular force field, which represents the potential energy as a function of atomic positions, and studying molecular properties while disregarding electron movements. The energy expression is composed of classical equations, including the harmonic oscillator equation, to describe the energy related to bond stretching, angle bending, bond rotation, and intermolecular forces. The typical parameter sets are Merck molecular force field 94 (MMFF94), molecular mechanics 2 (MM2) and molecular mechanics 3 (MM3). As electrons are not explicitly considered for in the classical molecular mechanics, large systems consist of thousands atoms or more such as proteins, drugs and enzymes can be simulated to estimate conformational flexibility and relative stability. Later, molecular mechanics methods are extended to molecular dynamics to simulate the nuclear motion within a molecule at various time and positions by adopting quantum mechanics approximation.

The semi-empirical method is an approach based on quantum mechanics that eliminates electronic integration and incorporates exchange correlation effects and

empirical parameters to minimize errors in approximations. It simplifies mathematical equations by combining quantum mechanics techniques with real lab data (Feller, 1996). Semi-empirical method is limited to the study of valence electron behaviour as they interact more readily with other molecules. The calculation of inner orbitals involves adding empirical data obtained from experiments. This method is suitable for studying the behaviour of molecules in a solvent and can calculate molecules with up to 1000 atoms. The semi-empirical method employs three main parameters: The Austin model 1 (AM1) predicts heat of formation, the parametric method 3 (PM3) is well-suited for organic systems, and the intermediate neglect of differential overlap methods (INDO).

Quantum mechanics can be classified into two groups which are Hartree-Fock method and density functional theory (DFT). The simplest wave function method is the Hartree-Fock (HF), in which neglecting the Coulombic electron repulsion explicitly, hence taking the average effect of multi-electron wave function using mean field approximation to calculate the total energy of the molecule (Chuvylkin et al., 2005). The common basis sets used are Slater type orbitals and Gaussian type orbitals. The lack of electron correlation affecting the exact kinetic barriers and description of intramolecular forces such as London dispersion force. Later, the improved quality of HF methods introduced largely extended basis sets such as coupled cluster theory (CC) and configuration interaction (CI) that include electron correlation. However, the advanced calculation of post-HF methods is considerably computationally costly, and their greater approximation makes them more suitable for large systems.

Density functional theory (DFT), in which the total energy is expressed in terms of the total electron density, leads to effective approximations using a Hamiltonian model (Baerends et al., 1997). In general, to study the properties of solid materials,

microscopy investigations must be conducted on atoms by analysing electron behaviour. Knowing the position of electrons can describe energy changes in the atom. In quantum mechanics, researchers face difficulties in calculating each electron in an atom due to the high number of interaction between particles. Thus, the most plausible way to analyse electrons is by using the density of particles in a particular region. The common parameter sets used to estimate electron density are local density approximation (LDA), generalized gradient approximation (GGA), and hyper-GGA. DFT calculations give very good qualitative results and can provide increasingly accurate quantitative results in small systems consisting of approximately 100 atoms. The main methods of computational chemistry are summarized in **Table 3.1**.

Table 3.1: Classification of Computational Chemistry Methods

Method	Description	Size of system
Molecular mechanics	Uses classical mechanics force fields to explain and interpret the behaviour of atoms and molecules.	Up to 100, 000 atoms
Semi-empirical	A quantum mechanics-based approach that simplifies equations with the use of empirical parameters.	Up to 1000 atoms
Quantum mechanics	The total energy is expressed in terms of the total electron density.	Up to 100 atoms

The Kohn-Hohenberg and Kohn-Sham are the backbones of DFT development in 1960s (Kohn et al., 1996). Their mathematical theorems are proven to solve the many-body problems successfully (Sholl et al., 2009). Initially, Kohn and Hohenberg postulated that a functional of electron density could represent the ground state energy obtained from the Schrodinger equation (Sholl, 2009). Essentially, the ground state dictates all properties such as energy and wavefunction. However, the theory lacks a comprehensive explanation of the function and requires further elaboration Later, Hohenberg and Kohn developed the idea that the total energy of a system can be minimized by using the exact electron density. (Sholl, 2009). This provided a method

for determining the relevant electron density once the actual functional form was established. The functional must be varied until the electron density reaches the minimum energy level, and the true functional is then formed. To express the correct electron density, Kohn and Sham proposed that the solution of the set of equations should be included, where each equation in the set accounts for a single electron (Kohanoff, 2006).

$$\varepsilon_i \psi_i(r) = \frac{h^2}{m}\nabla^2 + V(r) + V_H(r) + V_{XC}(r)]\psi_i(r) \quad (3)$$

ε_i is the energy of the *i*-th molecular orbital, ψ_i (r) is the wavefunction of the *i*-th molecular orbital. *h* is Planck's constant, *m* is the mass of an electron, ∇^2 is the Laplacian operator, V(r) is the potential energy of the electron due to its interaction with the nuclei, V_H(r) is the Hartree potential energy of the electron due to its interaction with all other electrons, and V_{XC}(r) is the exchange-correlation potential energy of the electron due to its interaction with all other electrons in the system.

The DFT approach has high accuracy for structural and electronic studies since it solves the exact Schrodinger equation using exchange-correlation functional. However, the selection of the right basis set and exchange correlation are very crucial to determine the accuracy because DFT approach acquires high computational hardware and plenty of time. This matter will be further discussed in next subtopic.

3.1 Exchange-Correlation

The development of accurate functional to represent the complete functional stay as the main topic in the most crucial fields of scientific research. The origin of energy functional emerge by local density approximation (LDA) that assumes the density is the same everywhere hence the calculation becomes simple but not accurate

(Sholl, 2009). To overcome this problem, a generalized gradient approximation (GGA) is constructed that used both the local electron density and the local gradient in the electron density. Later in 1990, rapid theoretical progress produce hybrid functional with the mixture of Hartree-Fock (HF) exchange correlation. The remodelling by hybrid functional improves the estimation of atomic energy, bond length, vibration frequency and others. The application of hybrid functional can be seen through several methods such as Becke, three-parameters, Lee-Yang-Parr (B3LYP) and Minnesota 06 (M06-2X) exchange correlation functional. The hybrid functional which is B3LYP has been recognized as the most popular method for DFT calculations because its less approximation on metal complex compounds and high accuracy are very close to experimental results (Becke, 2014). The Jacob's ladder approach has summarized the DFT functional according to the metaphor of Perdew and Schmidt (Gomes, 2013). As moving from LDA to GGA, metaGGA, and hybrid functional, the accuracy of the DFT calculation increases, but at the cost of greater computational complexity and decreased simplicity.

3.2 Basis Set

In computational modelling, a basis function or basis set is a set of functions used to represent the electronic wave function in DFT or HF codes, in order to convert partial differential equations into algebraic equations for efficient implementation on a computer. The minimal basis sets offered by the Gaussian program is the STO-3G consists of slater-type and Gaussian-type atomic orbitals (Hehre et al., 1969). Since valence orbitals of atoms are more affected by forming a bond than the inner (core) orbitals, split-valence basis sets were introduced to represent more basis functions to describe valence orbitals. Later, more basis functions are assigned to describe

polarization and diffusion functions of the whole molecule such as Pople's basis sets. The main basis sets are 3-211+G(d,p), 6-31++G(d,p), and 6-311++G(d,p) widely used to describe the structural, electronic and optical properties of organic compound (Sakthi et al., 2017).

For transition metals in third to higher row elements, effective core potential (ECP) approaches are used to treat inner orbitals electrons as average potential rather than actual particles (Wadt et al., 1985). This pseudopotential effects are very important in describing heavy atoms accurately while saving computational effort. The common basis sets for transition metals is Los Alamos National Laboratory 2 double-zeta (LANL2DZ) that consist of double zeta (two polarization functions) quality and the overall combination of ECP effect (Dunning, 1977).

Based on previous research Pople's basis sets and ECP approaches are more reliable in treating metal complexes (Bahsis et al., 2020). Therefore, this study will conduct preliminary study on several basis sets to identify which functional producing the most stable optimized structure with lowest total energy.

3.3 Polarizable Continuum Model

Solvation is the interaction of a solvent with the dissolved solute, which leads to the stabilization of the solute species in the solution. The physical interaction between solute and solvent molecules which is electrostatic force influences the structure, spectra and other properties of solute (Jelle et al., 2018). Therefore, researchers built a solvation model when modelling reaction to estimate the solvent effects on the behaviours of solute in a realistic environment.

To the present day, the major approaches in computational chemistry regarding solvent effects are:

i- Explicit model: consider molecular details of each solvent molecule

ii- Implicit model: treat solvents as a continuum medium (Zhang et al., 2017)

iii- Hybrid model: apply quantum and classical calculation to different parts of a single molecule

The implicit solvation model has been frequently used over the years to calculate molecular free energy and describes a thermodynamic property which is the dielectric constant of solution accurately with affordable computation cost (Chen et al., 2019). The solvation process begins with the creation of a cavity then, turns on dispersion and repulsion forces and finally turning on electrostatic forces. The solute molecule is embedded in a cavity surrounded by a continuous medium where the solvent is modelled as a continuous mass rather than as discrete particles.

Among the continuum models, the polarizable continuum model (PCM) formulated by (Miertuš et al., 1981) is one of the most established approaches to describe molecular solute. The integral equation formalism of polarizable continuum model (IEFPCM) is the latest version of PCM by accounting for the effect of the outlying charge and it leads the way to correct reaction potential inside the solute cavity (Mennucci, 2012). The IEFPCM method must be specified in software package with the self-consistent reaction field (SCRF) method and the dielectric constant value for accounting the effect of polarizable solvent. **Table 3.2** summarize the solvents used in this research.

Table 3.2: Solvents list and dielectric constant value, ε

Solvent	Dielectric value, ε (Frisch et al., 2016)
Water	78.3553
Acetonitrile	35.688
Methanol	32.613
Chloroform	4.7113
Toluene	2.37
Hexane	1.8819

3.4 Hardware

The computer used in this simulation is hp model: Intel® Xeon® E-22233 Processor (3.6 GHz base frequency, up to 3.9 GHz with Intel® Turbo Boost Technology, 8.25 MB cache, 4 cores), with installed RAM of 16.00 GB and 64-bit of Windows operating system.

3.5 Software

Theoretical simulations of the Pd(II) tetraaza macrocyclic complex are conducted using DFT and its extension, TDDFT, implemented by the Gaussian 16 package. Gaussian input files will be created using GaussView 6 as a graphical interface. The field of theoretical chemistry has made numerous contributions to the understanding of molecular phenomena through computational models and algorithms used by academic and industrial software packages. Density functional theory has been translated into quantum mechanics modelling by many software platforms, such as the Gaussian 16 package.

The Gaussian 16 is an electronic structure program used to investigate chemical problems with a wide range of complexity using modest computer software. Generally, computational time increases with the accuracy of the calculation, size of the system, and hardware specifications. The level of accuracy also depends on the level of

exchange-correlation and basis sets used. Therefore, it is crucial to find a balance between the method and equipment to achieve a reasonable level of accuracy within stipulated time frames.

3.6 Ground State Calculation

This section shows the geometry optimization and energy calculation of tetraaza macrocyclic ligand and Pd(II) tetraaza macrocyclic complex by DFT method in gas phase. The calculated bond parameters, MEPS, and NBO analysis provide an explanation for the structural and electronic properties of the tetraaza macrocyclic ligand and its complex. The steps are:

1. Protonated tetraaza macrocyclic ligand is constructed using GaussView.
2. The structure is optimized by applying 'Opt+Freq' job type in order to get lowest energy surface plot and zero imaginary frequency.
3. The computational variables are summarized in **Table 3.3** and the input is saved as *gjf* file.
4. Once calculation is completed, convergence is achieved, the results of bond parameters is saved in *log* file and MEPS visualization is saved in *chk* file.
5. Next, job type 'energy' is selected and keyword 'pop=nbo' is added on optimized structure of the ligand to observe the NBO analysis. The result is saved in *log* file.
6. Steps 1-5 are repeated for Pd(II) complex structure to complete the ground state calculation.

Table 3.3: Gaussian16 Input of Tetraaza Macrocylic Ligand and Its Complex

Compound	Method	Functional	Basis set	Charge
Ligand	DFT/Ground state	B3LYP	STO-3G 3211G ++** 6-311G ++ **	+2
Pd(II) complex	DFT/Ground state	B3LYP	LanL2DZ	+2

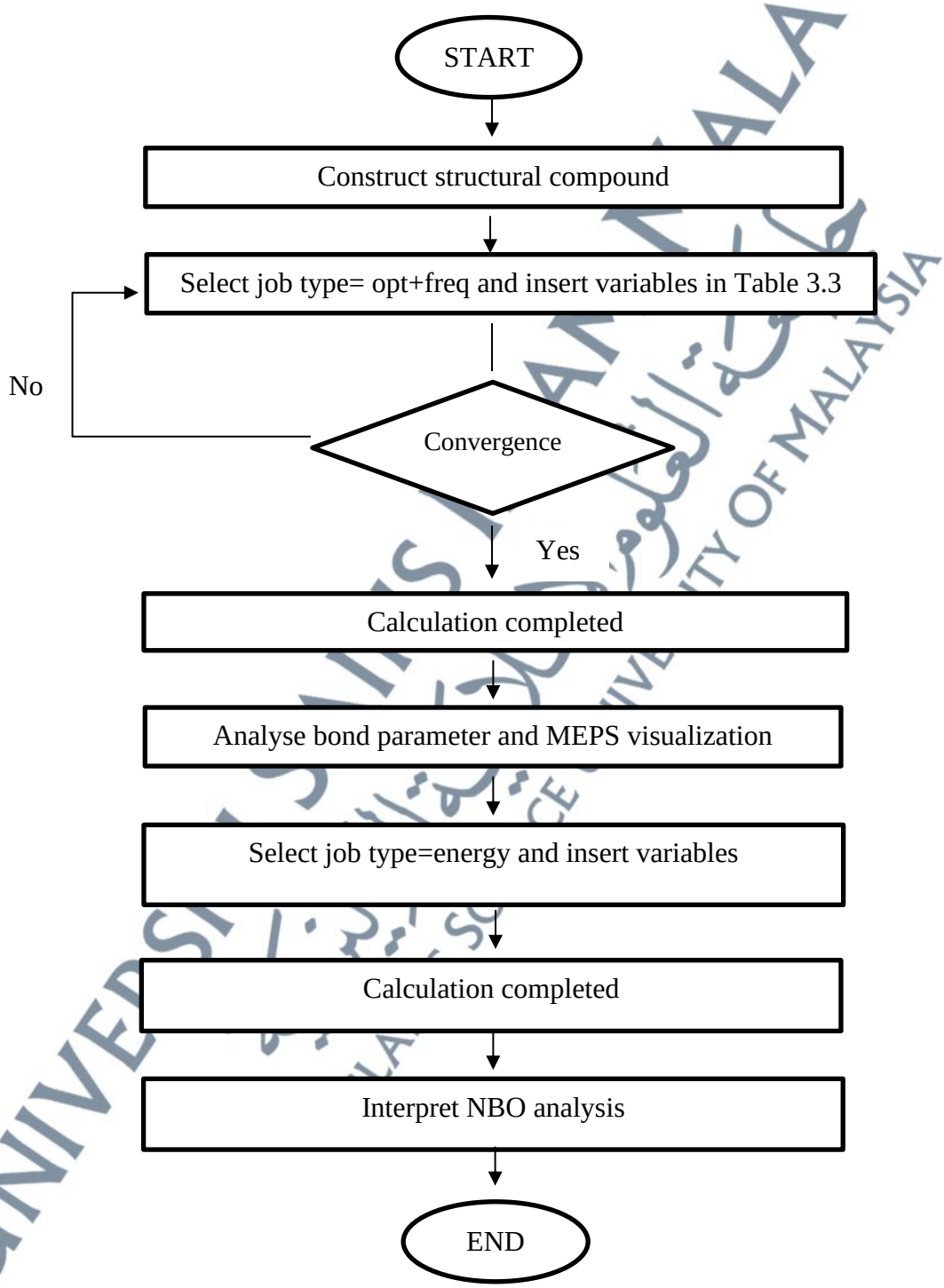

Figure 3.1: Flowchart of the Ground State Calculation

3.7 Excited State Calculation

This section shows the optimization, frequency and energy calculation of Pd(II) tetraaza macrocyclic complex by TD-DFT method in gas phase. From the calculations, the frontier molecular orbital, UV-Vis spectrum, and NLO properties explain the optical properties of the Pd(II) complex. The steps are:

1. Pd(II) complex is constructed using GaussView.
2. The structure is optimized by applying 'Opt' job type in order to get lowest energy surface plot at excited state.
3. The computational variables are summarized in **Table 3.4** and the input is save as *gjf* file.
4. Once calculation is completed, FMO visualization is saved in *chk* file
5. Next, job type 'Frequency' is selected and keyword 'polar' is added to observe NLO activity.
6. Once calculation is completed, NLO properties is saved in *log* file.
7. Next, job type 'Energy' is selected to get UV-vis spectrum. The result is saved in *log* file.

Table 3.4: Gaussian16 Input of Pd(II) Complex At Excited State

Compound	Method	Functional	Basis set	Charge
Pd(II) complex	TD-SCF/DFT	B3LYP	LanL2DZ	+2

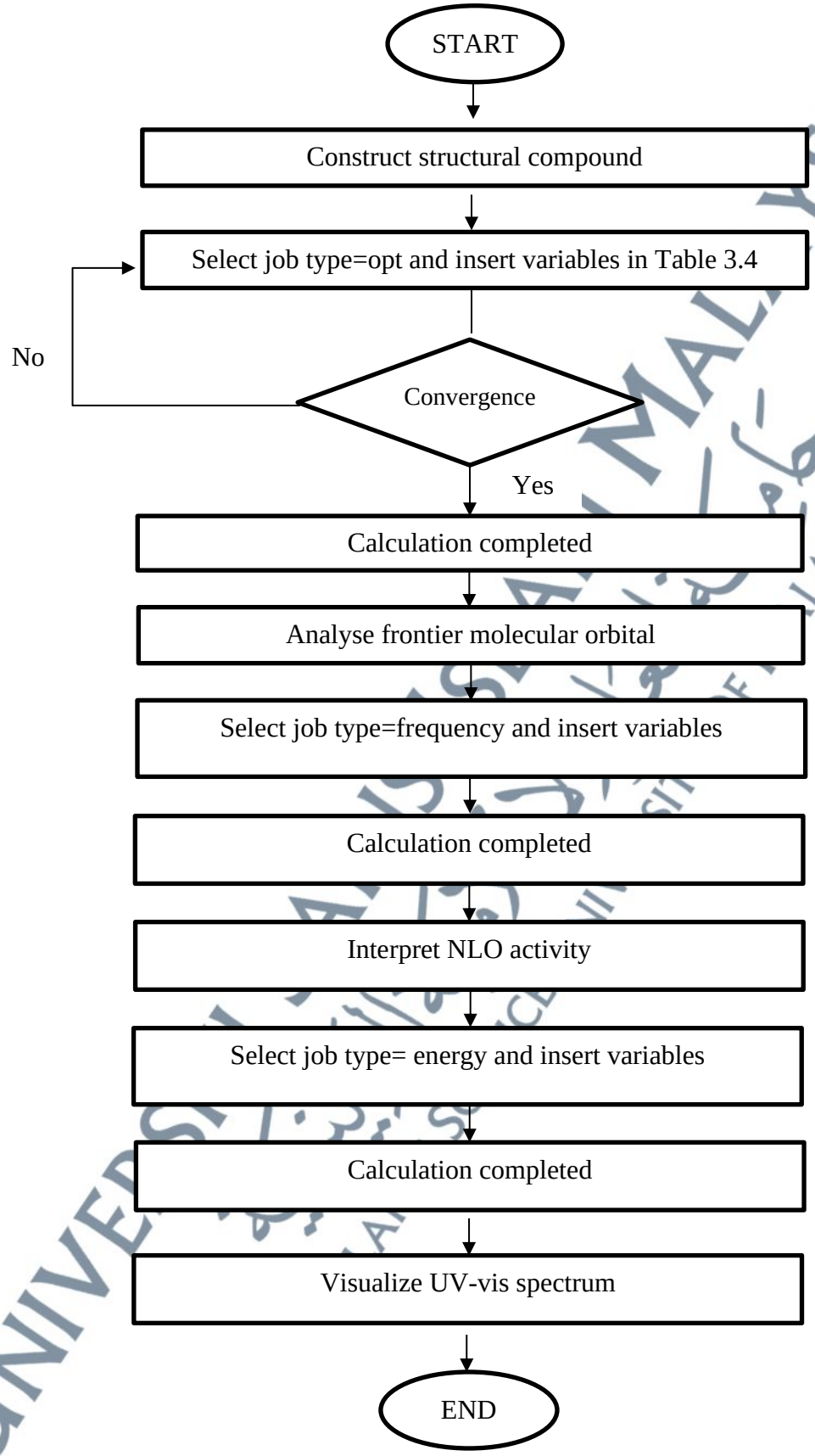

Figure 3.2: Flowchart of the Excited State Calculation

3.8 Solvation Model Calculation

This section presents the optimization, frequency, and energy calculations of the Pd(II) tetraaza macrocyclic complex using the TD-DFT method in a solvent environment. The calculations provide insights into the optical properties of the Pd(II) complex, including its frontier molecular orbital, UV-Vis spectrum, and NLO properties. The steps are:

1. Pd(II) complex is constructed using GaussView.
2. The structure is optimized by applying 'Opt' job type in order to get lowest energy surface plot in acetonitrile environment in ground state.
3. The computational variables are summarized in **Table 3.3** and the input is save as *gjf* file.
4. Steps 1-3 are repeated for different solvent which are methanol and water.
5. The structure is optimized by applying 'Opt' job type in order to get lowest energy surface plot in acetonitrile environment in excited state.
6. The computational variables are summarized in **Table 3.5** and the input is saved as *gjf* file.
7. Once calculation is completed, FMO visualization is saved in *chk* file
8. Next, job type 'Frequency' is selected and keyword 'polar' is added to observe NLO activity.
9. Once calculation is completed, NLO properties is saved in *log* file.
10. Next, job type 'Energy' is selected to get UV-vis spectrum. The result is saved in *log* file.
11. Steps 1-7 are repeated for different solvent which are hexane, chloroform, methanol and water.

Table 3.5: Gaussian16 Input of Pd(II) Complex in Solvent Phase

Compound	Method	Functional	Basis set	Charge	Model
Pd(II) complex	DFT/ Ground state	B3LYP	LanL2DZ	+2	IEF-PCM
Pd(II) complex	TD-SCF/DFT	B3LYP	LanL2DZ	+2	IEF-PCM

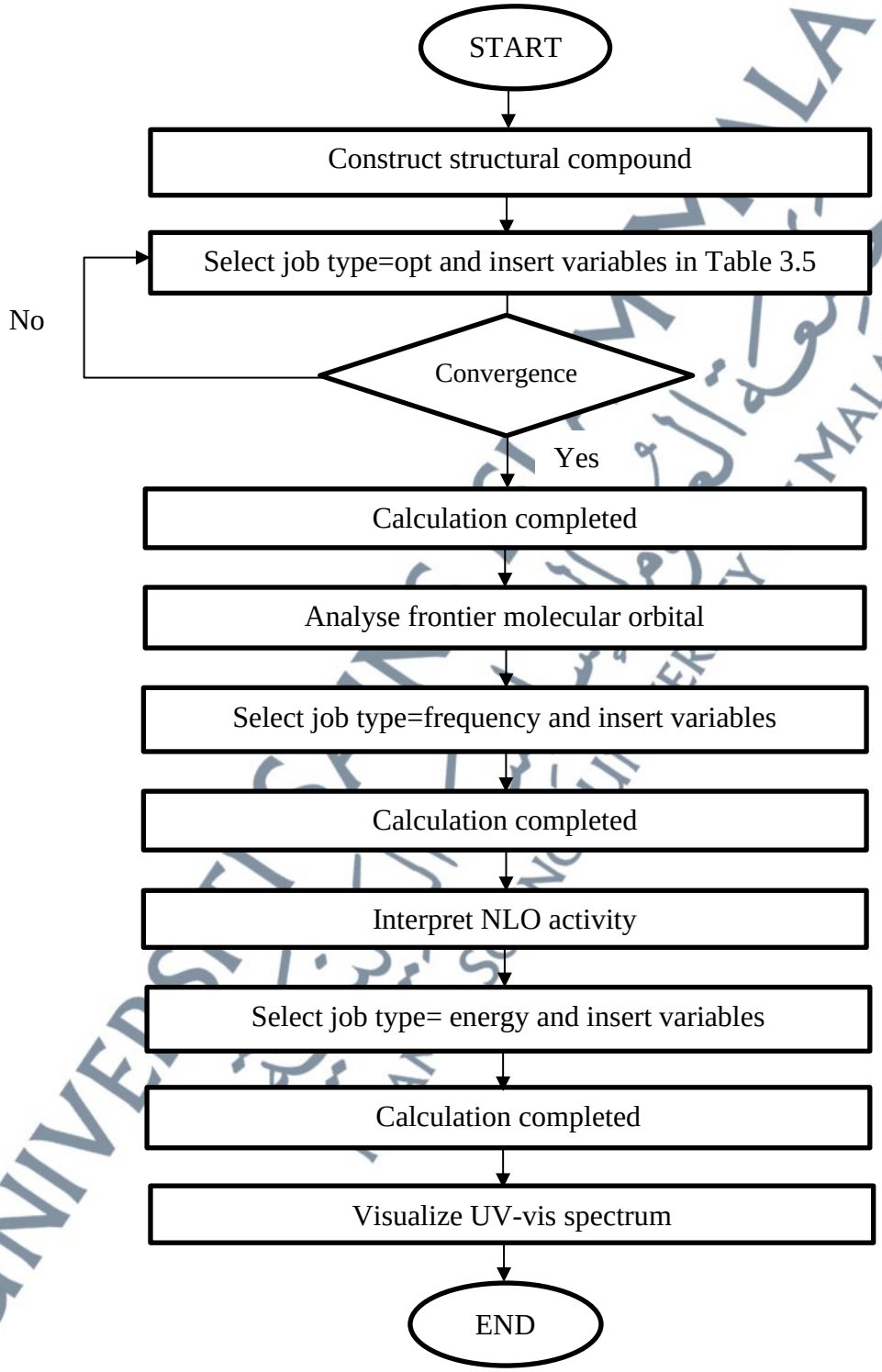

Figure 3.3: Flowchart of the Solvation Model Calculation